Radiation losses in intersecting optical waveguides

Niraj Agrawal[a] and L. McCaughan
Department of Electrical and Computer Engineering, University of Wisconsin, Madison, Wisconsin 53706

(Received 31 October 1988; accepted for publication 20 February 1989)

A systematic theory for radiation losses in intersecting optical waveguides is presented for the first time. These losses are shown to arise from a coupling between guided and radiation fields of the individual waveguides. The existence of a doubly peaked radiation loss characteristic with respect to the intersection angle is predicted for single-Δn intersecting waveguides and verified experimentally. A method for reducing the radiation losses by a simple modification of the intersection region is also discussed.

I. INTRODUCTION

Intersecting waveguides are routinely used in the design of a variety of circuit elements for integrated optics because of their novel topological features. Small and large intersection angles offer the possibility of making switches[1] and crossovers,[2] respectively. A proper understanding of the mechanism of radiation losses in intersecting waveguides is of vital importance for the development of more complex optical circuits. The previous theory for intersecting waveguides is based on the concept of interference between the modes of this composite waveguide structure.[1] Such an approach tacitly assumes the absence of radiation losses. The coupling between intersecting waveguides is also treated by a numerical technique known as the beam propagation method.[3] However, the calculated behavior of radiation losses is not even in qualitative agreement with the experiments.[2,4]

We have recently developed a unified theory which is able to account for recent experimental data on intersecting waveguides.[4-7] In this theory the two waveguides interact by scattering the fields of each other in a self-consistent manner. The effect of source fields generated in such a sequence of multiple scattering interactions can be evaluated by using Green's function for the individual waveguides. In a later section the construction and physical significance of the Green's function for an optical waveguide is described and its spectrum is shown to consist of both guided $g(.)$ and radiation $r(.)$ fields/modes. The coupling between two optical waveguides, therefore, consists of the following type of interactions: $g(1) \leftrightarrow g(2)$, $g(1) \leftrightarrow r(2)$, $r(1) \leftrightarrow g(2)$, and $r(1) \leftrightarrow r(2)$. The coupling between guided modes of intersecting waveguides has already been described in considerable detail.[5] In this paper an extension of the multiple scattering analysis to include the coupling between guided and radiation modes of intersecting waveguides, which is responsible for radiation losses, is reported. The nature of calculated radiation losses is in good agreement with the experimental measurements.[2,4] Finally, properties of fractional-Δn intersecting waveguides as low-loss structures is also discussed.

II. MULTIPLE SCATTERING ANALYSIS OF INTERSECTING WAVEGUIDES: AN OPERATOR FORMALISM

The wave equation for the transverse electric (TE) mode of intersecting waveguides ($\partial/\partial x = 0$, $\nabla_t^2 \equiv \partial^2/\partial y^2 + \partial^2/\partial z^2$) with a harmonic time dependence $\exp(-i\omega t)$ reduces to

$$[\nabla_t^2 + \omega^2 \mu \epsilon(y,z)] E_x(y,z) = 0. \tag{1}$$

The dielectric permittivity of the medium is given by

$$\epsilon(y,z) = \epsilon_s + \epsilon_1(y,z) + \epsilon_2(y,z) + \iota(y,z), \tag{2}$$

where ϵ_s pertains to the substrate, $\epsilon_{1,2}(y,z)$ represent the two intersecting single-mode waveguides, and $\iota(y,z)$ is used to incorporate an arbitrary scattering inhomogeneity in the intersection region (see Fig. 1). The total electric field $E_x(y,z)$ is decomposed in terms of fields $E_{x,i}(y,z)$ associated with the two waveguides with $i = 1,2$. The latter, in turn, are expressed as a sum of fields due to an infinite sequence of scattering interactions as

$$E_{x,i}(y,z) = \sum_{n=0}^{\infty} E_{x,i}^{(n)}(y,z), \tag{3}$$

where the superscript within the parentheses denotes the order of scattering interaction.

A guided wave is launched from the left of the junction at infinity in waveguide 1. The fields in the absence of coupling between the waveguides 1 and 2 are

$$E_{x,1}^{(0)}(y,z) = \Psi_1(y,z), \tag{4a}$$

$$E_{x,2}^{(0)}(y,z) = 0, \tag{4b}$$

where $\Psi_{1,2}$ represent the normalized eigenfunctions (TE_0) of the individual waveguides. However, in the presence of a

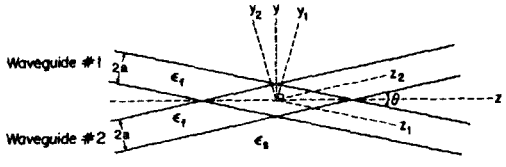

FIG. 1. Schematic diagram of the coordinate axes for the analysis of intersecting waveguides.

[a] Present address: IBM Research Division, Almaden Research Center, 650 Harry Road, San Jose, CA 95120-6099.

 0021-8979/89/124509-08$02.40

coupling between the two waveguides, the nth-order scattered fields $E_{x,i}^{(n)}(y,z)$ which are generated in sequence ..., $E_{x,2}^{(n)}(y,z)$, $E_{x,1}^{(n)}(y,z)$, ... for $n \geqslant 1$, can be expressed in terms of Green's function G_i of the individual waveguides with $i = 1,2$ as follows[5]:

$$E_{x,2}^{(n)}(y,z) = \frac{i\omega}{4}\int\int [\epsilon_2(y',z') + \iota(y',z')] \times E_{x,1}^{(n-1)}(y',z') G_2(y,z;y',z') dy'\, dz', \tag{5a}$$

$$E_{x,1}^{(n)}(y,z) = \frac{i\omega}{4}\int\int [\epsilon_1(y',z') + \iota(y',z')] \times E_{x,2}^{(n)}(y',z') G_1(y,z;y',z') dy'\, dz'. \tag{5b}$$

The Green's function $G_i(y,z;y',z')$ provides a complete description of fields generated at an arbitrary observation point (y,z) due to a source point at (y',z'). It is shown in the next section that the Green's function can be written as a sum of guided and radiation fields as

$$G_i(y,z;y',z') = G_i^{\text{gui}}(y,z;y',z') + G_i^{\text{rad}}(y,z;y',z'). \tag{6}$$

Two scattering operators $\mathbf{W}_2$ and $\mathbf{W}_1$ are defined such that Eqs. (5a) and (5b) can be written in a compact manner as

$$E_{x,2}^{(n)}(y,z) = \mathbf{W}_2 E_{x,1}^{(n-1)}(y,z), \tag{7a}$$

$$E_{x,1}^{(n)}(y,z) = \mathbf{W}_1 E_{x,2}^{(n)}(y,z). \tag{7b}$$

Equations (7a) and (7b) are rewritten as the following recurrence relations:

$$E_{x,2}^{(n+1)}(y,z) = \mathbf{W}_2\mathbf{W}_1 E_{x,2}^{(n)}(y,z), \tag{8a}$$

$$E_{x,1}^{(n+1)}(y,z) = \mathbf{W}_1\mathbf{W}_2 E_{x,1}^{(n)}(y,z). \tag{8b}$$

Moreover, the expressions for $E_{x,2}^{(n)}$ and $E_{x,1}^{(n)}$ in terms of the incident fields [see Eqs. (4) and (7)] become

$$E_{x,2}^{(n)}(y,z) = (\mathbf{W}_2\mathbf{W}_1)^{n-1}\mathbf{W}_2\Psi_1(y,z), \tag{9a}$$

$$E_{x,1}^{(n)}(y,z) = (\mathbf{W}_1\mathbf{W}_2)^{n}\Psi_1(y,z). \tag{9b}$$

Note that the number of times (multiplicity) the scattering operators occur in the expressions for the nth-order scattered fields $E_{x,2}^{(n)}$ and $E_{x,1}^{(n)}$ are given by $2n-1$ and $2n$, respectively. Finally, the scattering operator $\mathbf{W}_i$ with $i = 1,2$ is split into suboperators $\mathbf{U}_i$ (guided) and $\mathbf{V}_i$ (radiation) in order to account for Eq. (6) as follows:

$$\mathbf{W}_i = \mathbf{U}_i + \mathbf{V}_i. \tag{10}$$

III. GREEN'S FUNCTION FOR AN OPTICAL WAVEGUIDE

In the multiple scattering analysis of intersecting waveguides, the solution to the wave equations obtained in different orders of scattering interaction is expressed in terms of the Green's function for the individual waveguides [see Eqs. (4) and (5)]. In this section, the Green's function for an optical waveguide is constructed by a method similar to that of Collin.[8] The Green's function for a step-index optical waveguide is defined as

$$[\nabla_t^2 + \omega^2\mu\epsilon(y,z)]\, G(y,z;y',z') = i4\omega\mu\delta(y-y',z-z'), \tag{11a}$$

where

$$\epsilon(y,z) = \begin{cases} \epsilon_f & \text{if } -a \leqslant y \leqslant +a. \\ \epsilon_s & \text{otherwise.} \end{cases} \tag{11b}$$

The wave equation (11) is converted to an ordinary differential equation in y by taking its Fourier transform in the z coordinate as follows:

$$\left(\frac{d^2}{dy^2} + (\omega^2\mu\epsilon_f - \zeta^2)\right)\tilde{G}(y,\zeta;y',z') = i4\omega\mu\delta(y-y')e^{-i\zeta z'} \quad \text{for } |y| \leqslant a, \tag{12a}$$

$$\left(\frac{d^2}{dy^2} + (\omega^2\mu\epsilon_s - \zeta^2)\right)\tilde{G}(y,\zeta;y',z') = 0 \quad \text{for } |y| > a, \tag{12b}$$

where ζ is the Fourier transform variable and the source point (y',z') is assumed to be inside the waveguide. Since the Green's function defined by Eq. (11) corresponds to the TE mode, the boundary conditions on its Fourier transform are (i) $\tilde{G}$ continuous and $d\tilde{G}/dy$ discontinuous at $y = y'$ and (ii) $\tilde{G}$ continuous and $d\tilde{G}/dy$ continuous at $y = \pm a$. The discontinuity in $d\tilde{G}/dy$ at $y = y'$ is obtained by integrating Eq. (12) around the source point. Matching the fields at source point $(y = y')$ and boundaries $(y = \pm a)$ of the waveguide, the Fourier transform of the Green's function is obtained as

$$\tilde{G}(y,\zeta;y',z') = i2\omega\mu\left(\frac{1}{\xi D_e}\cos(\xi y')e^{ip(y-a)} - \frac{1}{\xi D_o}\sin(\xi y')e^{ip(y-a)}\right)e^{-i\zeta z'} \quad \text{for } +a \leqslant y < \infty, \tag{13a}$$

$$\tilde{G}(y,\zeta;y',z') = i2\omega\mu\left(\frac{D_o}{\xi D_e}\cos(\xi y')\cos(\xi y) - \frac{D_e}{\xi D_o}\sin(\xi y')\sin(\xi y) - \frac{1}{\xi}\sin(\xi y')\cos(\xi y) + \frac{1}{\xi}\cos(\xi y')\sin(\xi y)\right)e^{-i\zeta z'} \quad \text{for } -a \leqslant y' < y \leqslant +a, \tag{13b}$$

$$\tilde{G}(y,\zeta;y'z') = i2\omega\mu\left(\frac{D_o}{\xi D_e}\cos(\xi y')\cos(\xi y) - \frac{D_e}{\xi D_o}\sin(\xi y')\sin(\xi y) + \frac{1}{\xi}\sin(\xi y')\cos(\xi y) - \frac{1}{\xi}\cos(\xi y')\sin(\xi y)\right)e^{-i\zeta z'} \quad \text{for } -a \leqslant y < y' \leqslant +a, \tag{13c}$$

$$\tilde{G}(y,\zeta;y',z') = i2\omega\mu\left(\frac{1}{\xi D_e}\cos(\xi y')e^{-i\rho(y+a)} + \frac{1}{\xi D_o}\sin(\xi y')e^{-i\rho(y+a)}\right)e^{-i\zeta z'}$$

$$\text{for } -\infty < y \leqslant -a, \tag{13d}$$

where

$$D_e = \sin(\xi a) + (i\rho/\xi)\cos(\xi a), \tag{13e}$$

$$D_o = \cos(\xi a) - (i\rho/\xi)\sin(\xi a). \tag{13f}$$

The constants ξ and ρ are defined by

$$\xi^2 = \omega^2\mu\epsilon_f - \zeta^2 \equiv k_f^2 - \zeta^2, \tag{14a}$$

$$\rho^2 = \omega^2\mu\epsilon_s - \zeta^2 \equiv k_s^2 - \zeta^2. \tag{14b}$$

In order to obtain the Green's function G in real space, its Fourier transform $\tilde{G}$ is inverted using the following relation:

$$G(y,z;y',z') = \frac{1}{2\pi}\int_C \tilde{G}(y,\zeta;y',z')e^{i\zeta z}\,d\zeta. \tag{15}$$

The Fourier transform $\tilde{G}$ is a multiple valued function of ζ because of the two branches of ρ with branch points at $\zeta = \pm k_s$. The complex ζ plane must be cut by branch lines running from the branch points to infinity in order to provide a passage between the two Riemann sheets [see Fig. 2(a)]. The contour of integration C in the ζ plane is chosen such that G has a proper behavior (which means that it remains finite) at infinity ($|y| \to \infty$). It follows from the time dependence $e^{-i\omega t}$ and Eqs. (13a) and (13d) that this requires Im $(\rho) \geqslant 0$. Moreover, the branch of ρ such that $\mathrm{Re}(\rho) \geqslant 0$, gives outward going waves for $|y| \geqslant a$ and hence satisfies the Sommerfeld's radiation condition.[9] The Fourier transform $\tilde{G}$ has a discrete distribution of poles in the ζ plane. These poles when obtained by solving the dispersion relations $D_e = 0$ and $D_o = 0$ for ζ in the interval $k_s < |\zeta| < k_f$ correspond to even and odd guided modes of the waveguide, respectively. Since the contour of integration cannot be closed in the upper or lower half plane for the choice of branch cuts specified in Fig. 2(a), it is convenient to transform the variable of integration using

$$\zeta = k_s \cos q, \tag{16a}$$

$$\rho = k_s \sin q, \tag{16b}$$

where ζ, ρ, and q are complex variables. Equation (16) represents a mapping of the ζ plane into a strip of q plane [see Fig. 2(b)]. The proper (shaded) and improper (unshaded) sheets of the Riemann surface map into a connected strip given by $-\pi/2 \leqslant \mathrm{Re}(q) < 3\pi/2$. In the transformed q plane there are no branch cuts and the Fourier transform $\tilde{G}$ is analytic everywhere except in the neighborhood of its poles. Therefore, the contour of integration is deformed from C to steepest descent contour (*SDC*) without affecting the value of the Fourier integral. The significance of the new contour is explained later in this section. The line integral along *SDC* in the q plane is broken into paths which are comprised of circles warped around the poles plus the rest of the contour *SDC* [see Fig. 2(b)].

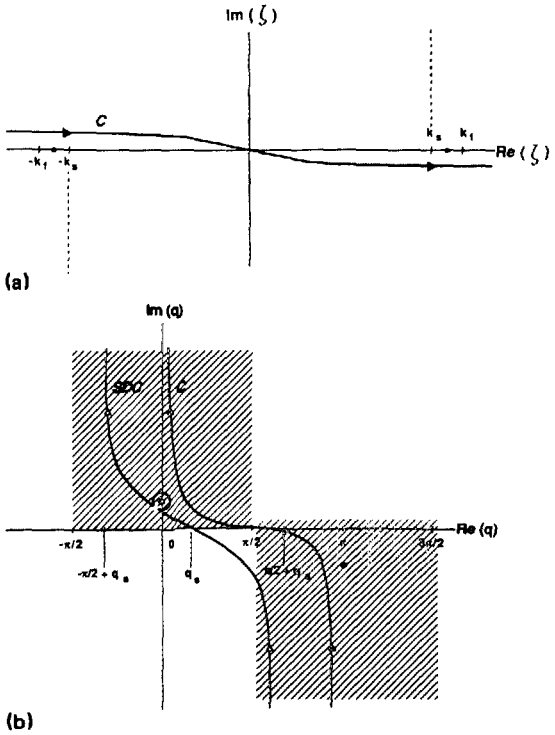

FIG. 2. (a) Contour of integration C in ζ plane along which the Green's function has a proper behavior at infinity and the Sommerfeld's radiation condition is satisfied. (b) Mapping of proper (shaded) and improper (unshaded) sheets of the Riemann surface into a connected strip in the q plane and deformation of original contour C into the steepest descent contour (SDC).

The contribution of the poles can be evaluated using the residue theorem. Thus, the guided part of the Green's function for a single-mode waveguide is obtained in terms of its normalized (unit power) eigenfunction $\Psi(y,z)$ as

$$G^{\mathrm{gui}}(y,z;y',z') = \Psi^*(y',z')\Psi(y,z) \quad \text{for } z \geqslant z', \tag{17a}$$

$$G^{\mathrm{gui}}(y,z;y',z') = \Psi(y',z')\Psi^*(y,z) \quad \text{for } z \leqslant z'. \tag{17b}$$

The eigenfunction in turn is given by

$$\Psi(y,z) = \frac{\sqrt{2\omega\mu}\,e^{-\gamma(y-a)}e^{i\beta z}}{\sqrt{\beta}\sqrt{(a+1/\gamma)}\sqrt{(1+\gamma^2/\alpha^2)}}$$

$$\text{for } +a \leqslant y < \infty, \tag{18a}$$

$$\Psi(y,z) = \frac{\sqrt{2\omega\mu}\,\cos(\alpha y)e^{i\beta z}}{\sqrt{\beta}\sqrt{(a+1/\gamma)}} \quad \text{for } -a \leqslant y \leqslant +a, \tag{18b}$$

$$\Psi(y,z) = \frac{\sqrt{2\omega\mu}\,e^{\gamma(y+a)}e^{i\beta z}}{\sqrt{\beta}\sqrt{(a+1/\gamma)}\sqrt{(1+\gamma^2/\alpha^2)}}$$

$$\text{for } -\infty < y \leqslant -a. \tag{18c}$$

The following relations are satisfied by the constants α,β,γ:

$$\alpha^2 = \omega^2\mu\epsilon_f - \beta^2, \tag{19a}$$

$$\gamma^2 = \beta^2 - \omega^2\mu\epsilon_s, \tag{19b}$$

$$\gamma = \alpha\tan(\alpha a). \tag{19c}$$

The Fourier integral along rest of the contour represents radiation fields and is too complicated to evaluate for all points in space [see Eqs. (13) and (15)]. However, in the far zone it can be simplified by the asymptotic technique known as saddle-point method. In order to employ this method we

convert to cylindrical coordinates for fields above $(y \geqslant a; \eta \equiv 1)$ and below $(y \leqslant -a; \eta \equiv -1)$ the waveguide using

$$z = r\cos\phi, \tag{20a}$$

$$y - \eta a = r\sin\phi. \tag{20b}$$

Substituting Eqs. (16) and (20) in Eq. (13), the expression for Green's function ($|y| \geqslant a$) becomes

$$G(r,\phi;y',z') = \int_C [g_e(q) - \eta g_o(q)]\, e^{irk_s\cos(q-\eta\phi)} \times(-k_s\sin q)dq, \tag{21a}$$

where

$$g_e(q) = \frac{i\omega\mu}{\pi}\left(\frac{\cos(\xi y')e^{-i\xi z'}}{\xi D_e}\right)_{\zeta = k_s\cos q}, \tag{21b}$$

$$g_o(q) = \frac{i\omega\mu}{\pi}\left(\frac{\sin(\xi y')e^{-i\xi z'}}{\xi D_o}\right)_{\zeta = k_s\cos q}. \tag{21c}$$

The complex argument f of the exponential term in Eq. (21a) is approximated as

$$f(q) \equiv irk_s\cos(q-\eta\phi) \approx f(q_s) + f'(q_s)(q-q_s) + f''(q_s)(q-q_s)^2/2. \tag{22}$$

The value of saddle point q_s is obtained from the relation $f'(q_s) = 0$ which implies $q_s = \eta\phi$. The *SDC* contour which also passes through the saddle point is defined by $f_2(q) \equiv \mathrm{Im}[f(q) - f(q_s)] = 0$. Note that along *SDC* the function $f_1(q) \equiv \mathrm{Re}[f(q) - f(q_s)]$ is negative and varies at a maximum rate away from the saddle point. Therefore, the entire contribution to the line integral (apart from that due to poles) comes from a small neighborhood of the saddle point as $r \to \infty$. In this way the radiation part of the Green's function is obtained in the far zone from Eq. (21) as

$$G^{\mathrm{rad}}(r,\phi;y',z') = \sqrt{2\pi k_s/r}\, e^{i(k_s r - \pi/4)} \times [g_e(\eta\phi) - \eta g_o(\eta\phi)]\sin(\eta\phi), \tag{23}$$

where the terms which vary slower than $r^{-1/2}$ are ignored because they do not contribute to the power flow across a closed cylindrical surface at infinity. Note that except in the far zone this method is not applicable for the evaluation of radiation fields.

A ray optical interpretation of the Green's function can be obtained as follows (see Fig. 3). Substituting Eqs. (13) and (14) in Eq. (15) shows that the radiation fields inside and outside the waveguide can be viewed as a superposition of plane waves/rays with wave vectors given by

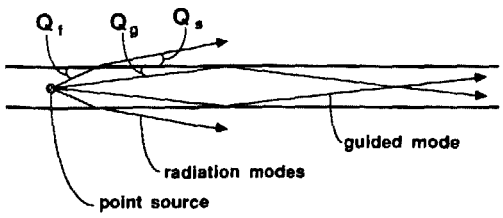

FIG. 3. Ray optical interpretation of the Green's function for a slab waveguide in terms of guided and radiation modes.

$$\mathbf{K}_f = (\zeta, \pm\xi) \equiv (k_f\cos Q_f, \pm k_f\sin Q_f), \tag{24a}$$

$$\mathbf{K}_s = (\zeta, \pm\rho) \equiv (k_s\cos Q_s, \pm k_s\sin Q_s). \tag{24b}$$

In a similar manner the guided fields inside the waveguide are represented [see Eqs. (18) and (19)] as

$$\mathbf{K}_g = (\beta, \pm\alpha) \equiv (k_f\cos Q_g, \pm k_f\sin Q_g). \tag{25}$$

The ray angle for guided fields outside the waveguide is imaginary. Note that the ray angles Q_f, Q_s in Eq. (24) and Q_g in Eq. (25) assume continuous and discrete values, respectively. The consistency between Eqs. (24a) and (24b) requires

$$k_f\cos Q_f = k_s\cos Q_s, \tag{26}$$

which is simply the Snell's law of refraction. The critical angle Q_c for the film-substrate interface is given by $\cos^{-1}(k_s/k_f)$. Thus, the radiation fields can be interpreted in terms of optical rays ($Q_f > Q_c$) which refract out from film into the substrate and the guided fields as rays ($Q_g < Q_c$) which are total internally reflected within the waveguide. As a numerical example, $Q_g = 2.33°$ and $Q_c = 3.77°$ is obtained for waveguide parameters, half width $a = 2\ \mu m$, substrate index $n_s = 2.300$, and film index $n_f = 2.305$ corresponding to the single-mode titanium indiffused waveguides in lithium niobate at $\lambda = 1.3\ \mu m$. Finally, it should be noted that the duality between real (r,ϕ) and momentum (k_s, Q_s) space variables allows a description of radiation fields outside the waveguide in terms of either angle ϕ or ray angle Q_s.

IV. SCATTERING OF LIGHT INTO RADIATION FIELDS

An exact evaluation of expressions for $E_{x,2}$ and $E_{x,1}$ given by Eqs. (3)–(10) is not practical. The electric field associated with waveguide 2 in the first order of scattering interaction (Born approximation) is given by Eqs. (9) and (10) for $n = 1$ as

$$E^{(1)}_{x,2}(y_2,z_2) = \mathbf{W}_2\Psi_1(y_1,z_1) = (\mathbf{U}_2 + \mathbf{V}_2)\Psi_1(y_1,z_1). \tag{27}$$

Beyond this order, the electric field associated with waveguides 2 and 1 can be obtained from the fields previously scattered into the respective waveguides by a successive application of the composite operators $\mathbf{W}_i\mathbf{W}_j$ with $i = 2, j = 1$ and $i = 1, j = 2$ [see Eqs. (8a) and (8b)]. The action of these operators on an arbitrary operand field f is expressed using Eq. (10) as

$$\mathbf{W}_i\mathbf{W}_j f = (\mathbf{U}_i\mathbf{U}_j + \mathbf{V}_i\mathbf{U}_j + \mathbf{U}_i\mathbf{V}_j + \mathbf{V}_i\mathbf{V}_j)f. \tag{28}$$

In the last two terms in Eq. (28) the radiation fields $\mathbf{V}_j f$, act as sources for subsequent scattering. Since evaluation of these terms requires knowledge of the radiation fields everywhere in space, it becomes difficult to proceed further to higher-order analyses. Therefore, in this paper we restrict our attention to a first-order analysis of scattering of light into radiation fields. Nevertheless, this simplified analysis provides valuable insights into the mechanism of radiation losses. Note that in case of low-loss waveguide structures the effect of source terms $\mathbf{V}_i\mathbf{U}_j f$, $\mathbf{U}_i\mathbf{V}_j f$, and $\mathbf{V}_i\mathbf{V}_j f$ can be ignored in calculations pertaining to coupling between guided modes.[5]

The radiation fields in the Born approximation are obtained from Eq. (27) as

$$E^{\text{rad}}_{x,2}(y_2,z_2) \approx \mathbf{V}_2 \Psi_1(y_1,z_1) = \frac{i\omega}{4}\int\int [\epsilon_2(y_2',z_2') + \iota(y_2',z_2')] \times \Psi_1(y_1',z_1') G^{\text{rad}}_2(y_2,z_2;y_2',z_2') dy_2' dz_2', \quad (29)$$

where the integral representation for the operator $\mathbf{V}_2$ is obtained from Eqs. (5)–(7) and (10). The integral in Eq. (29) can be performed in two equivalent ways depending on whether the expression for the Green's function is employed in real or momentum space. However, it is more convenient to use the momentum space representation due to the nature of limits of integration. Substituting Eqs. (13), (15), (16), and (20) for the Green's function in Eq. (29), the radiation fields above ($y_2 \geqslant a; \eta \equiv 1$) and below ($y_2 \leqslant -a; \eta \equiv -1$) the waveguide 2 are given in cylindrical coordinates as

$$\lim_{r\to\infty} E^{\text{rad}}_{x,2}(r,\phi) = \int_C [I_e(q) - \eta I_o(q)] \times e^{irk_s \cos(q-\eta\phi)}(-k_s \sin q) dq, \quad (30a)$$

where the overlap integrals between guided and radiation fields are defined as

$$I_e(\zeta) = \frac{\omega^2\mu}{4\pi}\int\int [\epsilon_2(y_2',z_2') + \iota(y_2',z_2')] \times \Psi_1(y_1',z_1') \frac{\cos(\xi y_2') e^{-i\zeta z_2'}}{\xi D_e} dy_2' dz_2', \quad (30b)$$

$$I_o(\zeta) = -\frac{\omega^2\mu}{4\pi}\int\int [\epsilon_2(y_2',z_2') + \iota(y_2',z_2')] \times \Psi_1(y_1',z_1') \frac{\sin(\xi y_2') e^{-i\zeta z_2'}}{\xi D_o} dy_2' dz_2', \quad (30c)$$

$$I_{e,o}(q) \equiv I_{e,o}(\zeta)|_{\zeta = k_s \cos q}. \quad (30d)$$

Since an arbitrary scattering inhomogeneity ι can be selected in the intersection region, the present formalism allows consideration of a variety of waveguide structures. However, in what follows, the special case of fractional-Δn intersecting waveguides is considered. These waveguides are described in terms of fractional permittivity χ in the intersection region ($-a \leqslant y_{1,2} \leqslant +a$) as

$$\iota = (\chi - 2)(\epsilon_f - \epsilon_s) \equiv (\chi - 2)\Delta, \quad (31)$$

where the two extensively studied cases, namely, single-Δn and double-Δn intersecting waveguides correspond to $\chi = 1$ and 2, respectively. Substituting Eq. (31) in Eq. (30) the overlap integrals are readily evaluated to be

$$I_{e,o}(\zeta) = I^{ev}_{e,o}(\zeta) + (\chi - 1) I^{gd}_{e,o}(\zeta), \quad (32a)$$

where

$$I^{ev}_{e,o}(\zeta) = \sigma_{e,o} \frac{\omega^2\mu\Delta}{2\pi} \frac{\sqrt{2\omega\mu}}{\sqrt{\beta}\sqrt{(a+1/\gamma)}\sqrt{(1+\gamma^2/\alpha^2)}} \frac{1}{\xi D_{e,o}} \frac{1}{[\gamma^2 + (\beta\cot\theta - \zeta\csc\theta)^2]\sin\theta} \times \{\gamma\cos[(\beta\cot\theta - \zeta\csc\theta)a] - (\beta\cot\theta - \zeta\csc\theta)\sin[(\beta\cot\theta - \zeta\csc\theta)a]\} \times \left(\frac{\sin[(\xi + \zeta\cot\theta - \beta\csc\theta)a]}{(\xi + \zeta\cot\theta - \beta\csc\theta)} + \sigma^2_{e,o}\frac{\sin[(\xi - \zeta\cot\theta + \beta\csc\theta)a]}{(\xi - \zeta\cot\theta + \beta\csc\theta)}\right), \quad (32b)$$

$$I^{gd}_{e,o} = \sigma_{e,o}\frac{\omega^2\mu\Delta}{4\pi}\frac{\sqrt{2\omega\mu}}{\sqrt{\beta}\sqrt{(a+1/\gamma)}}\frac{1}{\xi D_{e,o}}\frac{1}{\sin\theta} \times \left(\frac{\sin[(\alpha + \beta\cot\theta - \zeta\csc\theta)a]}{(\alpha + \beta\cot\theta - \zeta\csc\theta)} + \frac{\sin[(\alpha - \beta\cot\theta + \zeta\csc\theta)a]}{(\alpha - \beta\cot\theta + \zeta\csc\theta)}\right) \times \left(\frac{\sin[(\xi + \zeta\cot\theta - \beta\csc\theta)a]}{(\xi + \zeta\cot\theta - \beta\csc\theta)} + \sigma^2_{e,o}\frac{\sin[(\xi - \zeta\cot\theta + \beta\csc\theta)a]}{(\xi - \zeta\cot\theta + \beta\csc\theta)}\right). \quad (32c)$$

A superscript on $I_{e,o}$ represents the fact that the overlap integral is between evanescent or guided fields of waveguide 1 with the radiation fields of waveguide 2. The constants σ_e and σ_o are given the complex values of $(-1,0)$ and $(0,1)$, respectively.

V. POYNTING VECTOR AND RELATED EXPRESSIONS

In the present case $(r,\phi,-x)$ constitutes a cylindrical coordinate system. The pertinent field components for the TE mode are E_{-x}, H_r, and H_ϕ, where

$$E_{-x} = -E_x, \quad (33a)$$

$$H_r = \frac{1}{i\omega\mu r}\frac{\partial E_{-x}}{\partial\phi}, \quad (33b)$$

$$H_\phi = -\frac{1}{i\omega\mu}\frac{\partial E_{-x}}{\partial r}. \quad (33c)$$

The power which flows out from a closed cylindrical surface at infinity is

$$P = \int S_r\, r d\phi, \quad (34a)$$

where the radial component of the Poynting vector is given by

$$S_r = \frac{1}{2}\text{Re}(-E_{-x}H^*_\phi). \quad (34b)$$

It follows from Eqs. (3), (9), and (10) that the total electric and magnetic fields associated with the two waveguides can

be expressed in terms of guided and radiation contributions as

$$E_{-x} = E^{\text{gui}}_{-x} + E^{\text{rad}}_{-x}, \tag{35a}$$

$$H_{\phi} = H^{\text{gui}}_{\phi} + H^{\text{rad}}_{\phi}. \tag{35b}$$

It can be readily shown that the cross terms between guided and radiation fields which are obtained by substituting Eq. (35) into Eq. (34) do not contribute to the power flow P in the asymptotic limit, therefore,

$$P = P^{\text{gui}} + P^{\text{rad}}. \tag{36}$$

In the present context the interest lies primarily in the radiation fields and the corresponding power. The radiation part of electric and magnetic fields is obtained in the Born approximation by first performing the Fourier integral in Eq. (30) by the saddle-point method and then using Eq. (33), respectively, as follows:

$$E^{\text{rad}}_{-x,2}(r,\phi) = -\sqrt{2\pi k_s/r}\, e^{i(k_s r - \pi/4)} \times [I_e(\eta\phi) - \eta I_o(\eta\phi)]\sin(\eta\phi), \tag{37a}$$

$$H^{\text{rad}}_{\phi,2}(r,\phi) = (k_s/\omega\mu)\sqrt{2\pi k_s/r}\, e^{i(k_s r - \pi/4)} \times [I_e(\eta\phi) - \eta I_o(\eta\phi)]\sin(\eta\phi) + O(r^{-3/2}), \tag{37b}$$

where the angle ϕ is measured with respect to the axis of waveguide 2. Next, a coupling coefficient between guided and radiation modes of the individual waveguides is defined as

$$J(\phi) = \sqrt{\pi k_s^2/\omega\mu}\,[I_e(\eta\phi) - \eta I_o(\eta\phi)]\sin(\eta\phi), \tag{38}$$

with $-\pi \leqslant \phi < \pi$ and $\eta = \pm 1$ for $\phi \gtrless 0$. Substituting the far-field expressions given by Eqs. (37a) and (37b) in Eq. (34) and using Eq. (38), the radiation pattern is obtained as

$$p^{\text{rad}}(\phi) = J(\phi)J^*(\phi). \tag{39}$$

Finally, the radiation pattern is integrated to evaluate the power lost due to radiation as

$$P^{\text{rad}} = \int_{-\pi}^{\pi} p^{\text{rad}}(\phi)\, d\phi. \tag{40}$$

VI. RESULTS AND DISCUSSION

Radiation loss phenomenon in single-Δn ($\chi = 1$) intersecting waveguides exhibits a doubly peaked characteristic with respect to the intersection angle as shown in Fig. 4. Such a behavior is not predicted by any theory of intersecting waveguides except the scattering analysis. It is evident that the theory and experiment[2,4] are in general agreement, the quantitative agreement being better at large intersection angles. [Note that the slab (TE) geometry is used to model the titanium-diffused channel (TM) waveguides in lithium niobate due to their equivalency.] These results can be interpreted as follows: At small intersection angles the interaction between guided modes of intersecting waveguides corresponds to several coupling lengths.[5] Therefore, the incident power is scattered into the guided and radiation modes of both waveguides. In order to incorporate these physical effects the higher-order scattering interactions

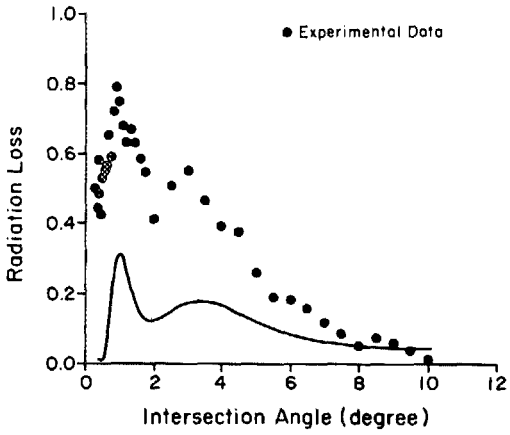

FIG. 4. Calculated (normalized to incident power) and measured (referenced to straight waveguide) radiation loss as a function of the intersection angle for single-Δn intersecting waveguides. The parameters $a = 2\ \mu$m, $n_s = 2.300$, and $n_f = 2.305$ are selected for numerical analysis so as to obtain single-mode slab waveguides (TE) at $\lambda = 1.3\ \mu$m. Measurements were made on titanium in-diffused lithium niobate intersecting channel (TM) waveguides (for experimental details, see Ref. 4).

must be considered [see Eqs. (9) and (10)]. A more detailed comparison of experimental results with scattering analysis at small angles is reported elsewhere.[4] However, at large intersection angles the strength of coupling between intersecting waveguides is greatly reduced so that a first-order scattering analysis is adequate.

The complexity of the closed-form expressions for the radiation coupling coefficients obtained by substituting Eq. (32) with $\zeta = k_s \cos(\eta\phi)$ and $\rho = k_s \sin(\eta\phi)$ in Eq. (38), makes it difficult to interpret them in an intuitive manner except for some general observations. The radiation coupling coefficient $J(\phi)$ for small and large intersection angles is shown in Figs. 5 and 6, respectively. The angle ϕ, or equivalently the ray angles Q_s, at which the radiation pattern vanishes are determined by zeros of $(\xi D_{e,o})^{-1}$ and the factors within large parentheses in Eqs. (32b) and (32c). Note that at small intersection angles the evanescent and guided contributions (corresponding to regions outside and inside the intersection region) to the radiation coupling coefficient are always of the opposite polarity and scaled in magnitude as compared to each other by roughly a constant factor. It is, therefore, possible to adjust the magnitude of $J^{gd}(\phi)$ relative to that of $J^{ev}(\phi)$ through the fractional permittivity χ so as to eliminate or reduce the coupling between guided and radiation modes [see Eqs. (32) and (38)]. The same is not true for large intersection angles. Moreover, the overall angular width of the radiation coupling coefficient increases with the intersection angle. The angular width, which is a measure of the stringency of phase matching condition between guided and radiation modes, is influenced by the argument $\Delta\Phi$ of sinc functions and is expressed in terms of various ray angles [see Eqs. (24), (25), and (32)] as

$$\Delta\Phi = (\xi \pm \zeta \cot\theta \mp \beta \csc\theta)a = k_f[\pm\cos(Q_f \mp \theta) \mp \cos Q_g]a \csc\theta, \tag{41a}$$

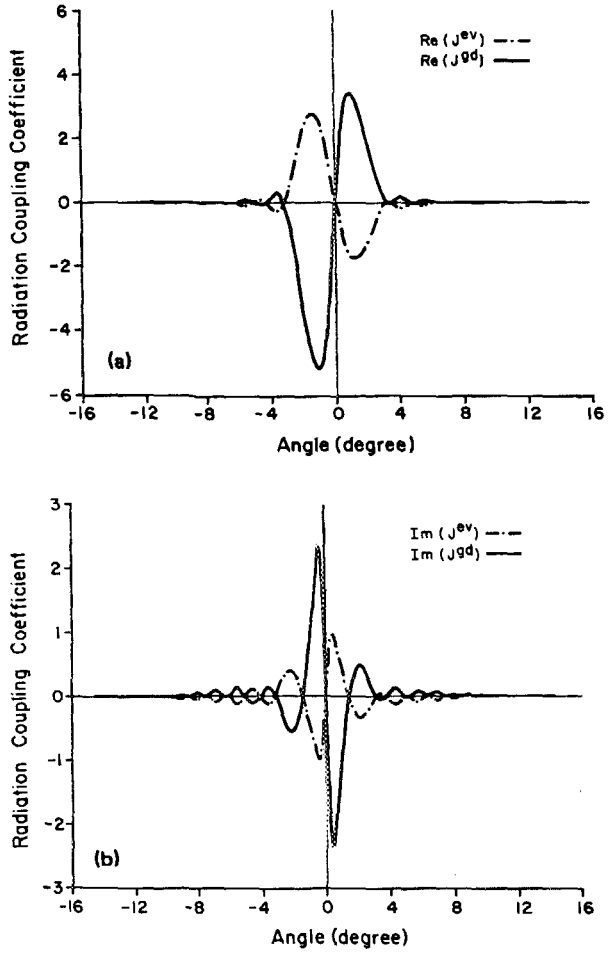

FIG. 5. (a) Real and (b) imaginary parts of radiation coupling coefficients as a function of angle (ϕ) for two waveguides intersecting at a small angle ($\theta = 1°$). The waveguide parameters are $a = 2$ μm, $n_s = 2.300$, and $n_f = 2.305$.

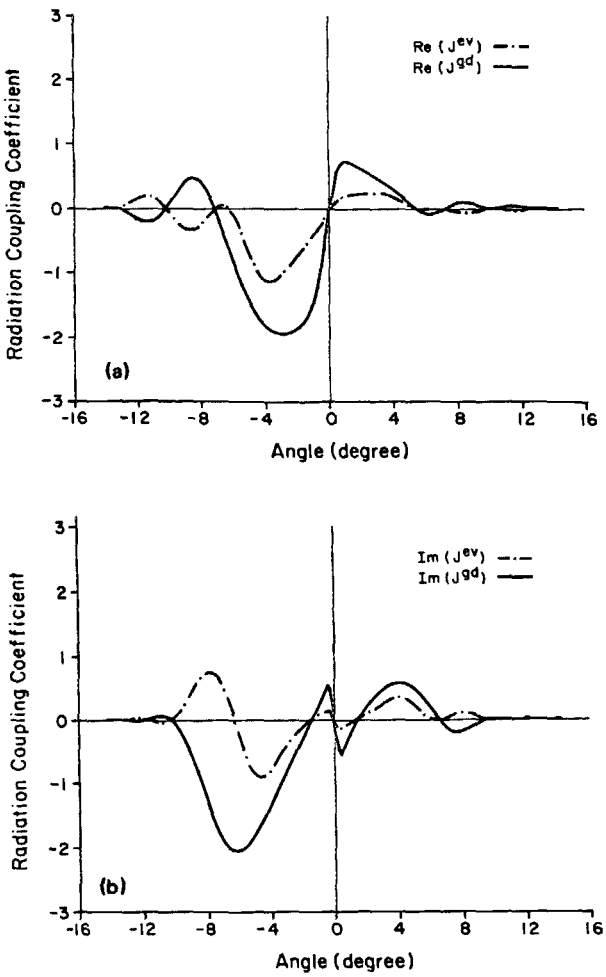

FIG. 6. (a) Real and (b) imaginary parts of radiation coupling coefficients as a function of angle (ϕ) for two waveguides intersecting at a large angle ($\theta = 5°$). The waveguide parameters are $a = 2$ μm, $n_s = 2.300$, and $n_f = 2.305$.

and

$$\Delta\Phi = (\alpha \pm \beta \cot\theta \mp \zeta \csc\theta)a$$
$$= k_f[\pm\cos(Q_g \mp \theta) \mp \cos Q_f]a \csc\theta. \quad (41b)$$

It follows from Eq. (41) that the effective length over which the wave vectors are mismatched is given by $a \csc\theta$. Therefore, the phase matching condition is relaxed with an increase in the intersection angle. Finally, we note that a sharply peaked radiation beam emanating from the junction of single-Δn intersecting waveguides has been observed[6] in accordance with the radiation pattern p^{rad} obtained through the present analysis and shown in Fig. 7. (The preliminary calculations reported earlier should be corrected by a factor of two due to numerical error. Compare Figs. 3 and 4 in Ref. 6 with Figs. 4 and 7 in this paper, respectively.)

A different version of this geometry, namely, double-Δn ($\chi = 2$) intersecting waveguides has been used to make optical switches with somewhat smaller losses.[1,10] There is no reason to assume that either single-Δn or double-Δn intersecting waveguides represent an optimum geometry with respect to providing low-loss waveguide structures. Therefore, we describe radiation losses in the generalized case of fractional-Δn intersecting waveguides. The radiation loss is shown in Figs. 8(a) and 8(b) as a function of fraction permittivity χ for two different values of mode confinement parameter ($V = 4\pi\sqrt{n_f^2 - n_s^2}\,a/\lambda$) for small and large intersection angles, respectively. Note that whereas the losses are drastically reduced in the fractional-Δn intersecting wave-

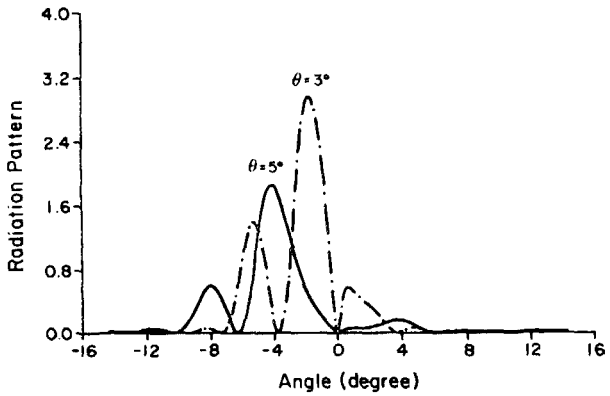

FIG. 7. Radiation pattern (p^{rad}) as a function of angle (ϕ) for intersecting waveguides with large intersection angles of 3 and 5°. The waveguide parameters are $a = 2$ μm, $n_s = 2.300$, and $n_f = 2.305$.

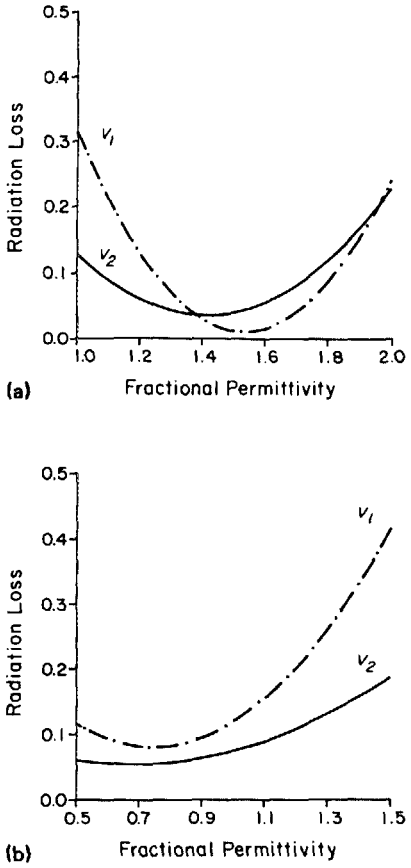

FIG. 8. Radiation loss as a function of fractional permittivity (χ) for intersecting waveguides with (a) small ($\theta = 1°$) and (b) large ($\theta = 5°$) intersection angles. The waveguide parameters are $a = 2\,\mu$m, $n_s = 2.300$, and (i) $n_f = 2.305$ ($V_1 = 2.93$) and (ii) $n_f = 2.303$ ($V_2 = 2.27$).

guides with small intersection angles, such effectiveness is not seen at large angles. In addition, the minimum loss attainable with respect to χ decreases (increases) with increasing V at small (large) angles. At a small intersection angle of 1°, a low-loss waveguide structure is obtained for a value of $\chi \simeq 1.54$ which is intermediate between single-Δn and double-Δn intersecting waveguides. In case of large intersection angles, a value of $\chi < 1$ yields the minimum radiation loss; however, the minimum value in this case is somewhat higher. These results follow directly from the interference between evanescent and guided contributions to radiation coupling coefficients depicted in Figs. 5 and 6.

VII. CONCLUDING REMARKS

A first-order scattering analysis is presented to evaluate radiation losses in intersecting waveguides under the assumption that they are sufficiently small. This approximation is not of concern because, in practice, the primary interest in integrated optics lies in low-loss waveguide structures. Note that a semiquantitative agreement between theory and experiment is demonstrated even in the presence of large radiation losses. Moreover, in the present formalism an arbitrary choice of scattering inhomogeneity $\iota(y,z)$ can be made in the vicinity of the intersection region. Such a generality allows consideration of index distributions for different waveguide structures with a wide variety of potential applications. However, it is important to recognize that there are some restrictions on $\iota(y,z)$ due to its strong influence on radiation losses as shown in Fig. 8.

Recently, there has been a considerable interest in the design of optical switch arrays.[11–13] Several different architectures with modest levels of integration have been demonstrated. In most applications it is important that the loss through the switch matrix be small as well as path independent. In order to fabricate such a switch array, both low-loss switches and crossovers are indispensable. In the case of directional couplers, this requirement translates into an increase in the length of the switch in order to accommodate the larger S bends,[14] which in turn reduces the packing density. However, as shown here, in an optical switch employing fractional-Δn intersecting waveguides with small angles, the radiation losses can be reduced without affecting its size. Although the fractional doping of the intersection region has a less dramatic effect in terms of making low-loss crossovers with large angles, other variations of intersecting waveguides may prove more effective towards this purpose.

ACKNOWLEDGMENTS

The authors are grateful to Professor J. A. Tataronis for valuable discussions. This research was supported by the National Science Foundation under Grant Nos. ECE-8508024 and EET-8802713.

[1] A. Neyer, Electron. Lett. **19**, 553 (1983).
[2] G. A. Bogert, Electron. Lett. **23**, 72 (1987).
[3] A. Neyer, W. Mevenkamp, L. Thylen, and B. Lagerström, IEEE J. Lightwave Technol. **LT-3**, 635 (1985).
[4] N. Agrawal and L. McCaughan Appl. Phys. Lett. **54**, 1669 (1989).
[5] N. Agrawal, L. McCaughan, and S. R. Seshadri, J. Appl. Phys. **62**, 2187 (1987).
[6] L. McCaughan, N. Agrawal, and G. A. Bogert, Appl. Phys. Lett. **51**, 1389 (1987).
[7] L. McCaughan, *Technical Digest of the Topical Meeting on Integrated and Guided-Wave Optics 1988*, Santa Fe, NM (Optical Society of America, Washington, DC, 1988), pp. 98–102.
[8] R. E. Collin, *Field Theory of Guided Waves* (McGraw-Hill, New York, 1960), Chap. 11, pp. 485–506.
[9] J. D. Jackson, *Classical Electrodynamics* (Wiley, New York, 1975), Chap. 9, pp. 427–432.
[10] E. E. Bergmann, L. McCaughan, and J. E. Watson, Appl. Opt. **23**, 3000 (1984).
[11] A. Neyer, W. Mevenkamp, and B. Kretzschmann, *Technical Digest of the Topical Meeting on Integrated and Guided-Wave Optics 1986*, Atlanta, GA (Optical Society of America, Washington, DC, 1986), pp. 4 and 5.
[12] P. J. Duthie and M. J. Wale, Electron. Lett. **24**, 594 (1988).
[13] G. A. Bogert, in *Photonic Switching*, edited by T. K. Gustafson and P. W. Smith (Springer, Berlin, 1988), pp. 67 and 68.
[14] W. J. Minford, S. K. Korotky, and R. C. Alferness, IEEE J. Quantum Electron. **QE-18**, 1802 (1982).